

# An ALMA survey of Sub-millimetre Galaxies in the Extended Chandra Deep Field South: Detection of [CII] at $z = 4.4$

A. M. Swinbank,<sup>1,\*</sup> A. Karim,<sup>1</sup> Ian Smail,<sup>1</sup> J. Hodge,<sup>2</sup> F. Walter,<sup>2</sup> F. Bertoldi,<sup>3</sup> A. D. Biggs,<sup>4</sup> C. de Breuck,<sup>4</sup> S. C. Chapman,<sup>5</sup> K. E. K Coppin,<sup>6</sup> P. Cox,<sup>7</sup> A. L. R. Danielson,<sup>1</sup> H. Dannerbauer,<sup>8</sup> R. J. Ivison,<sup>9,10</sup> T. R. Greve,<sup>11</sup> K. K. Knudsen,<sup>12</sup> K. M. Menten,<sup>3</sup> J. M. Simpson,<sup>1</sup> E. Schinnerer,<sup>2</sup> J. L. Wardlow,<sup>13</sup> A. Weiß,<sup>14</sup> P. van der Werf<sup>15</sup>

<sup>1</sup>*Institute for Computational Cosmology, Durham University, South Road, Durham, DH1 3LE, UK*

<sup>2</sup>*Max-Planck-Institut für Astronomie, Königstuhl 17, D-69117 Heidelberg, Germany*

<sup>3</sup>*Argelander-Institut of Astronomy, Bonn University, Auf dem Huegel 71, D-53121 Bonn, Germany*

<sup>4</sup>*European Southern Observatory, Karl-Schwarzschild Strasse 2, D-85748 Garching, Germany*

<sup>5</sup>*Institute of Astronomy, University of Cambridge, Madingley Road, Cambridge CB3 0HA*

<sup>6</sup>*Department of Physics, McGill University, 3600 Rue University, Montral, QC H3A 2T8, Canada*

<sup>7</sup>*Institut de Radioastronomie Millimétrique, 300 rue de la piscine, F-38406 Saint-Martin d'Hères, France*

<sup>8</sup>*Universität Wien, Institut für Astrophysik, Türkenschanzstraße 17, 1180 Wien, Austria*

<sup>9</sup>*UK Astronomy Technology Centre, Science and Technology Facilities Council, Royal Observatory, Blackford Hill, Edinburgh EH9 3HJ*

<sup>10</sup>*Institute for Astronomy, University of Edinburgh, Blackford Hill, Edinburgh EH9 3HJ*

<sup>11</sup>*University College London, Department of Physics & Astronomy, Gower Street, London, WC1E 6BT, UK*

<sup>12</sup>*Department of Earth and Space Sciences, Chalmers University of Technology, Onsala Space Observatory, SE-43992 Onsala, Sweden*

<sup>13</sup>*Department of Physics & Astronomy, University of California, Irvine, CA 92697, USA*

<sup>14</sup>*Leiden Observatory, Leiden University, PO Box 9513, 2300 RA Leiden, Netherlands*

\**Email: a.m.swinbank@dur.ac.uk*

27 June 2018

## ABSTRACT

We present ALMA 870- $\mu\text{m}$  (345 GHz) observations of two sub-millimetre galaxies (SMGs) drawn from an ALMA study of the 126 sub-millimeter sources from the LABOCA Extended *Chandra* Deep Field South Survey (LESS). The ALMA data identify the counterparts to these previously unidentified sub-millimeter sources and serendipitously detect bright emission lines in their spectra which we show are most likely to be [CII] 157.74  $\mu\text{m}$  emission yielding redshifts of  $z = 4.42$  and  $z = 4.44$ . This blind detection rate within the 7.5-GHz bandpass of ALMA is consistent with the previously derived photometric redshift distribution of SMGs and suggests a modest, but not dominant ( $\lesssim 25\%$ ), tail of 870- $\mu\text{m}$  selected SMGs at  $z \gtrsim 4$ . We find that the ratio of  $L_{[\text{CII}]} / L_{\text{FIR}}$  in these SMGs is much higher than seen for similarly far-infrared-luminous galaxies at  $z \sim 0$ , which is attributed to the more extended gas reservoirs in these high-redshift ULIRGs. Indeed, in one system we show that the [CII] emission shows hints of extended emission on  $\gtrsim 3$  kpc scales. Finally, we use the volume probed by our ALMA survey to show that the bright end of the [CII] luminosity function evolves strongly between  $z = 0$  and  $z \sim 4.4$ , reflecting the increased ISM cooling in galaxies as a result of their higher star-formation rates. These observations demonstrate that even with short integrations, ALMA is able to detect the dominant fine structure cooling lines from high-redshift ULIRGs, measure their energetics, spatially resolved properties and trace their evolution with redshift.

**Key words:** galaxies: starburst, galaxies: evolution, galaxies: high-redshift

## 1 INTRODUCTION

A significant fraction of the obscured star formation at  $z \gg 1$  arises from the most luminous galaxies (e.g. Blain et al. 1999; LeFloch et al. 2009): ultra-luminous infrared galaxies (ULIRGs; Sanders & Mirabel 1996) with bolometric luminosities of  $\gtrsim 10^{12-13} L_{\odot}$  and star-formation rates  $\gtrsim 100-1000 M_{\odot} \text{ yr}^{-1}$ . At high redshift, these galaxies are some of the brightest sources in the sub-millimetre wave-band and so are frequently called “sub-millimetre galaxies” (SMGs).

The spectral energy distribution (SED) of the dust emission in these luminous dusty galaxies has a Rayleigh-Jeans tail that produces a negative K-correction in the sub-millimetre wave-band, yielding a near constant flux density–luminosity dependence with redshift over the range  $z \sim 1-6$  (Blain et al. 2002). Although the volume density of the SMG population evolves rapidly with redshift, (showing a 1000-fold increase in the space density over the  $\sim 10$  Gyrs to  $z \sim 2.5$ ; Chapman et al. 2005), the volume density appears to subsequently decline above  $z \gtrsim 3$ . This decline is not a result of a reduction in their apparent flux density in the sub-millimetre, but a real reduction in the volume density of SMGs (Wardlow et al. 2011).

However, determining the precise strength of the decline in the SMG volume density requires locating the counterparts of high-redshift SMGs. This is problematic due to the poor resolution of single dish sub-millimetre maps, which means that SMGs have to be identified through correlations between their sub-millimetre emission and that in other wave-bands where higher spatial resolution is available (usually the radio and/or mid-infrared e.g. Ivison et al. 2002; Chapman et al. 2004; Ivison et al. 2007; Pope et al. 2006). These identifications are probabilistic as they rely on empirical correlations that have both significant scatter and which may evolve with redshift (e.g. Carilli & Yun 2000). Moreover, the SEDs in these other wave-bands have positive K-corrections and hence can miss the highest redshift counterparts. Indeed in sub-millimetre surveys typically 30–50% of SMGs lack “robust” counterparts in the radio or mid-infrared, and these may represent an unidentified tail of high-redshift SMGs (e.g. Biggs et al. 2011, see also Lindner et al. 2011). To circumvent this problem requires identifying SMGs using sub-/millimetre interferometers (e.g. Gear et al. 2000; Frayer et al. 2000), but until recently their sensitivity has been too low to locate large numbers of SMGs (e.g. Dannerbauer et al. 2002; Younger et al. 2007; Wang et al. 2011; Smolčić et al. 2012). However, with the commissioning of the Atacama Large Millimeter Array (ALMA), we can now construct the large samples of precisely-located SMGs needed to unambiguously study their properties and test galaxy formation models.

Whilst the bulk of the bolometric emission from SMGs is radiated through continuum emission from dust grains in the rest-frame far-infrared, superimposed on this are a series of narrow atomic and molecular emission lines. By far the strongest of these arise from the atomic fine-structure transitions of Carbon, Nitrogen and Oxygen in the far-infrared, along with weaker, but more commonly-studied molecular lines visible at millimetre wavelengths (e.g.  $^{12}\text{CO}$ , HCN). These bright emission lines are an important pathway by which the dense gas in these galaxies cools, and so provide a

unique tracers of the star-formation process in these galaxies.

The brightest and best-studied of the atomic lines in the far-infrared is the  $^2P_{3/2}-^2P_{1/2}$  fine structure line of singly ionised carbon at  $157.74\text{-}\mu\text{m}$  (here-after [CII]). Much of the [CII] emission from galaxies arises from the warm and dense photo-dissociation regions (PDRs) that form on the UV-illuminated surface of molecular clouds, although the [CII] flux from diffuse HII regions or from cool, diffuse interstellar gas can also be significant (e.g. Madden et al. 1993; Lord et al. 1996). The [CII] emission line therefore provides an indication of the gas content and the extent of the gas reservoir in a galaxy. Far-infrared surveys of low-redshift galaxies from the Kuiper Airborne Observatory and *ISO* have shown that the [CII] line can comprise  $\gtrsim 1\%$  of the total bolometric luminosity (Stacey et al. 1991; Braucher et al. 2008; Graciá-Carpio et al. 2011). This bright line is thus ideally suited for deriving redshifts for obscured galaxies and investigating their dynamics and star-formation properties.

Early searches for [CII], by necessity, focused on the highest-redshift far-infrared sources,  $z > 4$ , where the [CII] line is shifted into the atmospheric windows in the sub-millimetre (e.g. Ivison et al. 1998; Maiolino et al. 2005, 2009; Wagg et al. 2010). Most of these sources host powerful AGN (as well as being ULIRGs) and it was noted that their [CII] lines were weak relative to  $L_{\text{FIR}}$ , demonstrating the same behavior as seen in AGN-dominated ULIRGs in the local Universe. However, more recent observations of the [CII] emission in high redshift star-formation dominated ULIRGs has shown that the [CII] emission can be as bright as in local, low-luminosity galaxies,  $L_{[\text{CII}]} / L_{\text{FIR}} \sim 0.1-1\%$  (e.g. Hailey-Dunsheath et al. 2008; Ivison et al. 2010b; Stacey et al. 2010; Valtchanov et al. 2011). This has been interpreted as due to the lower ionisation field arising from more widely distributed star-formation activity within these systems, in contrast to the compact nuclear star formation seen in low-redshift ULIRGs (e.g. Sakamoto et al. 2008). The strength of [CII] (and other atomic lines), and its relative strength to the far-infrared luminosity can therefore be used to probe the physical properties of the interstellar medium in high-redshift galaxies.

We have recently undertaken an ALMA Cycle 0 study at  $870\mu\text{m}$  (345 GHz) of the 126 sub-millimeter sources located in the  $0.5^{\circ} \times 0.5^{\circ}$  LABOCA Extended *Chandra* Deep Field South Survey (“LESS”; Weiß et al. 2009), the most uniform sub-millimetre survey of its kind to date. These ALMA data yield unambiguous identifications for a large fraction of the sub-millimeter sources, directly pin-pointing the SMG responsible for the sub-millimetre emission to within  $< 0.2''$  (Hodge et al. 2012, in prep), without recourse to statistical radio/mid-infrared associations. In this letter, we present ALMA observations of two of the SMGs from our survey for which we are able to derive their redshifts from serendipitous identification of the [CII] emission line in the ALMA data-cubes. We use the data to measure the energetics of the dominant fine structure lines, search for spatially resolved velocity structure and to provide an estimate of the evolution of the [CII] luminosity function with redshift. We adopt a cosmology with  $\Omega_{\Lambda} = 0.73$ ,  $\Omega_m = 0.27$ , and  $H_0 = 72 \text{ km s}^{-1} \text{ Mpc}^{-1}$  in which  $1''$  corresponds to a physical scale of  $6.7 \text{ kpc}$  at  $z \sim 4.4$ .

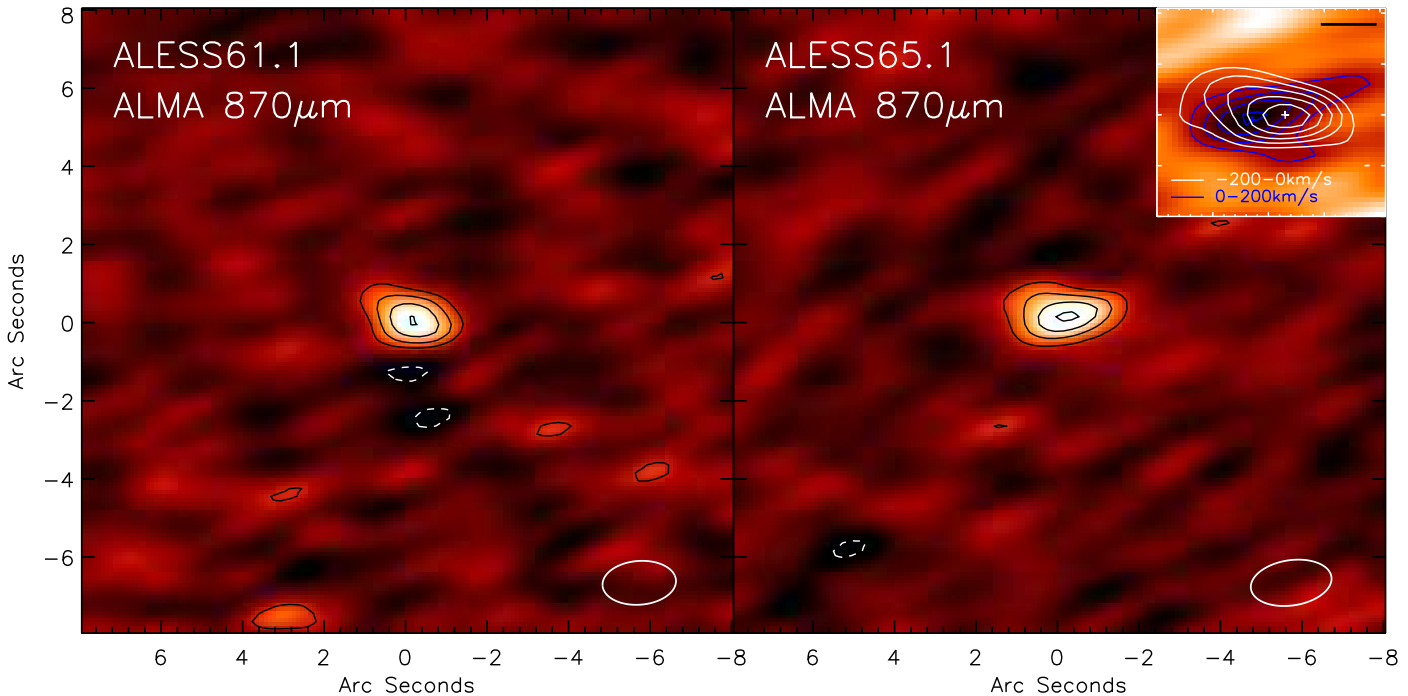


**Figure 1.** *Top:* 870 $\mu\text{m}$  (345 GHz) velocity integrated ALMA maps of LESS 61 and LESS 65 from the Band 7 ALMA observations in compact configuration (these maps include the continuum and emission lines and are naturally weighted). In both cases, we detect strong 870 $\mu\text{m}$  emission in both sub-millimeter sources associated with a single SMG. The r.m.s. noise in these maps is 0.44 and 0.42 mJy beam $^{-1}$  for LESS 61 and LESS 65 respectively. Contours denote  $\pm 3, 5, 7\dots\sigma$ . In each panel we also show the 50% contour of the synthesised beam which is approximately  $1.8'' \times 1.2''$  in both cases. These maps are centered at  $\alpha : 03\ 32\ 45.87$   $\delta : -28\ 00\ 23.3$  and  $\alpha : 03\ 32\ 52.26$   $\delta : -27\ 35\ 26.3$  for LESS 61 and LESS 65 respectively (Table 1). The inset in LESS 65 shows the velocity structure in the [CII] in this source. The colour scale shows the (continuum subtracted) velocity integrated cube between  $-210$ – $0$  km s $^{-1}$  with the blue contours at 2, 3, 4, 5... $\sigma$ . The white contours denote the velocity integrated emission  $0$ – $210$  km s $^{-1}$  (also at 2, 3, 4, 5... $\sigma$ ). The spatial offset between the blue-shifted and red-shifted emission in these two images is  $0.50 \pm 0.25''$  ( $3.3 \pm 1.7$  kpc). If this spatial and velocity offsets represents rotating gas reservoir, then we estimate a dynamical mass of  $M_{\text{dyn}} \sim 3.5 \times 10^{10} \sin^2(i) M_{\odot}$ . In this inset, the solid bar shows a scale of  $1''$ .

## 2 OBSERVATIONS AND REDUCTION

Observations of the 126 sub-millimeter sources in the LESS survey were obtained with ALMA at 345 GHz (Band 7) with a dual polarisation setup in the compact configuration, yielding a synthesised beam of  $\sim 1.8'' \times 1.2''$ . Our observations cover 7.5 GHz band-width, split between the upper- and lower-sidebands, 336.1–339.8 GHz and 348.1–351.9 GHz. The observations employed 15 antennae and data for these two sources were obtained between 2011 October and 2011 November in good conditions, PWV  $\lesssim 0.5$  mm. The primary beam of the ALMA dishes,  $\sim 18''$  FWHM at our observing frequency, is sufficient to encompass the error-circles of the SMGs from the LESS maps,  $\lesssim 5''$  (Weiß et al. 2009), even in confused situations. The observing frequency was selected to match the original LABOCA discovery map to ensure that the ALMA and LABOCA flux densities could be easily compared. Each galaxy was observed for a total of  $\sim 120$  seconds, with phase, bandpass and flux calibration based on J0403-360, J0538-440 and Mars, respectively. The data were processed with the Common Astronomy Software Application (CASA; McMullin et al. 2007), and we constructed both velocity integrated maps and datacubes with 62.5 MHz (54.5 km s $^{-1}$ ) binning. The velocity integrated continuum maps for the two sources discussed here reach noise levels of  $\sigma = 0.44$  and 0.42 mJy beam $^{-1}$  for LESS 61 and LESS 65 respectively. This is a factor  $\sim 3 \times$

more sensitive than the original LABOCA discovery map, while more critically the beam is  $\sim 150 \times$  smaller in area than that of LABOCA (with a corresponding reduction in the positional uncertainty of detected sources). In the datacubes, the r.m.s. sensitivity is  $\sim 3.8$  mJy beam $^{-1}$  per 54.5 km s $^{-1}$  (62.5 MHz) channel. The full catalog of the ALMA SMGs will be published in Hodge et al. (2012, in prep), whilst the ALMA 870 $\mu\text{m}$  counts and multi-wavelength properties of the ALMA SMGs will be published in Karim et al. (2012, in prep) and Simpson et al. (2012, in prep).

## 3 ANALYSIS AND DISCUSSION

Wardlow et al. (2011) derive a photometric redshift distribution for the statistically identified radio- and mid-infrared counterparts of the LESS sub-millimeter sources, deriving a median  $z = 2.5 \pm 0.5$ . Taking the errors on the redshifts into account, we expect  $3.5 \pm 0.5$  SMGs should have far-infrared fine structure lines (such as [CII] 157.74 $\mu\text{m}$ , [OI] 145 $\mu\text{m}$ , [NII] 122 $\mu\text{m}$  or [OIII] 88 $\mu\text{m}$ ) within the 7.5 GHz bandwidth of ALMA. By far the brightest of these lines in local ULIRGs is the [CII] emission line, with a median equivalent width  $\gtrsim 10 \times$  brighter than any of the other lines (Brauer et al. 2008). Focusing just on [CII], we expect  $1.5 \pm 0.5$  SMGs in our sample will have detectable [CII] emission in the ALMA band-pass, with corresponding redshift ranges of

**Table 1.** Co-ordinates and Photometry

	ALESS 61.1	ALESS 65.1
ID <sup>a</sup>	J033245.6–280025	J033252.4–273527
R.A. (ALMA) <sup>b</sup>	03 32 45.87	03 32 52.26
Dec. (ALMA) <sup>b</sup>	–28 00 23.3	–27 35 26.3
S <sub>870</sub> (LABOCA)	5.8 ± 1.2	5.9 ± 1.2
S <sub>870</sub> (ALMA) <sup>c</sup>	4.32 ± 0.44	4.24 ± 0.49
0.365 μm	< 1.2 × 10 <sup>−4</sup>	< 9.9 × 10 <sup>−5</sup>
0.350 μm	< 9.9 × 10 <sup>−5</sup>	< 9.9 × 10 <sup>−5</sup>
0.460 μm	< 5.7 × 10 <sup>−5</sup>	< 1.8 × 10 <sup>−4</sup>
0.538 μm	< 6.9 × 10 <sup>−5</sup>	< 3.6 × 10 <sup>−4</sup>
0.651 μm	< 6.3 × 10 <sup>−5</sup>	< 6.3 × 10 <sup>−5</sup>
0.833 μm	4.7 ± 1.1 × 10 <sup>−4</sup>	< 1.2 × 10 <sup>−3</sup>
0.850 μm	8.5 ± 1.0 × 10 <sup>−4</sup>	< 3.6 × 10 <sup>−4</sup>
0.903 μm	7.3 ± 1.6 × 10 <sup>−4</sup>	< 2.4 × 10 <sup>−3</sup>
2.2 μm	3.0 ± 0.3 × 10 <sup>−3</sup>	< 2.7 × 10 <sup>−3</sup>
3.6 μm	3.3 ± 0.3 × 10 <sup>−3</sup>	2.1 ± 0.2 × 10 <sup>−3</sup>
4.5 μm	3.9 ± 0.2 × 10 <sup>−3</sup>	1.4 ± 0.2 × 10 <sup>−3</sup>
5.8 μm	2.7 ± 1.0 × 10 <sup>−3</sup>	1.4 ± 1.0 × 10 <sup>−3</sup>
8.0 μm	5.4 ± 0.7 × 10 <sup>−3</sup>	3.0 ± 0.8 × 10 <sup>−3</sup>
24 μm	0.036 ± 0.002	< 0.006
250 μm	4.3 ± 1.5	< 2.7
350 μm	7.4 ± 1.6	7.6 ± 1.4
500 μm	10.2 ± 1.7	10.2 ± 1.5
1.4 GHz	< 0.025	< 0.025

Notes: All flux densities are in mJy and all limits are  $3\sigma$ .

<sup>a</sup> LESS ID from the LABOCA catalog in Weiß et al. (2009). <sup>b</sup> Co-ordinates in J2000. <sup>c</sup> The ALMA flux densities have been primary beam corrected (the primary beam corrections are a factor 1.12 and 1.04 for ALESS 61.1 and ALESS 65.1 respectively). The *BVRIZK*+IRAC photometry comprises VIMOS (*U*), MUSYC (*BVRIZ*), *HST* ( $z_{850\text{LP}}$ ); HAWK-I (*K*) and IRAC 3.6–8 μm imaging (see Wardlow et al. 2011, for details). The *Herschel* SPIRE photometry is measured using archival imaging and the photometry has been de-blended for nearby sources. The radio flux density limits are taken from the VLA 1.4 GHz imaging used in Biggs et al. (2011).

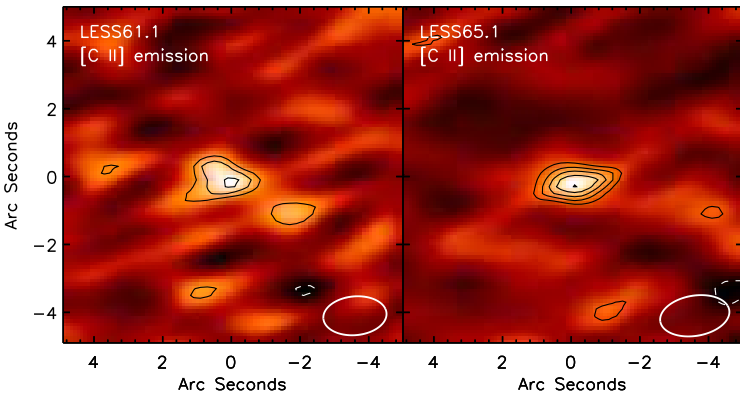


**Figure 2.** Continuum subtracted [CII] emission line maps of LESS 61.1 and LESS 65.1. These are generated by subtracting the continuum and then integrating the cube between  $\pm 2 \times \text{FWHM}$  of the emission line. In all panels the contours denote S/N levels denote  $\pm 3, 4, 5 \dots \sigma$ .

$z = 4.399\text{--}4.461$  and  $z = 4.590\text{--}4.656$  for the upper and lower-side bands.

As an initial step in our analysis of the ALMA maps of the LESS sub-millimeter sources, we exploit the frequency coverage of our observations to search for emission lines in the datacubes. For each  $>4\text{-}\sigma$  SMG in the velocity-integrated ALMA maps within the primary beam, we extract the spectra and search for emission lines by attempting to fit a Gaussian emission line profile to the spectrum, only accepting the fit if the  $\Delta\chi^2$  provides a significant improvement ( $\Delta\chi^2 > 25$ , or  $\sim 5\sigma$ ) over a continuum-only fit.

### 3.1 Source Identification

In two sub-millimeter sources, LESSJ033245.6–280025 and LESSJ033252.4–273527 (hereafter ALESS 61.1 and ALESS 65.1, respectively following the notation in Hodge et al. 2012, in prep), we identify bright emission lines with FWHM  $230 \pm 25$  and  $490 \pm 35 \text{ km s}^{-1}$  respectively in the spectra of these SMGs. The significance of the emission lines (integrated over the line) is  $S/N \sim 5.3$  and  $7.0$  for ALESS 61.1 and ALESS 65.1 respectively. In Fig. 1 we show the velocity-integrated (continuum plus line) ALMA maps of ALESS 61.1 and ALESS 65.1 while the spectra are shown in Fig. 3. To highlight the emission line detections in both ALMA SMGs, in Fig. 2 we also show the continuum subtracted emission line maps. In this figure, the map is made by integrating the continuum subtracted cube over  $\pm 2 \times \text{FWHM}$  of the emission line.

In both cases, the LABOCA 870 μm source is identified with a single high signal-to-noise ( $S/N \sim 8$ ) ALMA SMG in the velocity integrated maps that is located to within  $< 0.2''$  (after centroiding) and  $3\text{--}4''$  from their nominal LABOCA positions (Weiß et al. 2009). Biggs et al. (2011) could not identify robust or tentative counterparts for either of these sub-millimeter sources (see also Wardlow et al. 2011) as no SMGs were detected at 1.4 GHz ( $3\sigma \leq 25 \text{ mJy}$  at 1.4 GHz). Both sources are very faint in the *Herschel*/SPIRE imaging at 250, 350, and 500 μm (the SMGs are weakly detected after de-blending nearby sources using the 24 μm and radio as priors; Table 1). The ALMA maps reveal that ALESS 61.1 is associated with a weak 24 μm source that is also visible in the optical–mid-infrared, but ALESS 65.1 does not have any counterparts in the optical or near-infrared and is only detected weakly in the *Spitzer* IRAC imaging. Together, this suggest that these galaxies lie at  $z \gtrsim 3.5$  (Wardlow et al. 2011). With the current data, we find no evidence for strong gravitational lensing of either of these galaxies.

### 3.2 Line Identification

If the emission lines we identified are indeed [CII], then our data indicate redshifts of  $z = 4.419$  and  $z = 4.445$  for ALESS 61.1 and ALESS 65.1 respectively. The rest-frame equivalent widths of the emission lines are  $0.44 \pm 0.06 \mu\text{m}$  and  $1.12 \pm 0.15 \mu\text{m}$ , similar to the median equivalent width of [CII] in local LIRGs and ULIRGs ( $W_{\text{e},[\text{CII}]} = 0.76 \pm 0.06 \mu\text{m}$ ; Braucher et al. 2008). We note that in the 7.5 GHz spectral coverage at 345 GHz, the emission lines contribute 10–40% of the continuum emission in the velocity integrated cubes, as predicted by Smail et al. (2011).

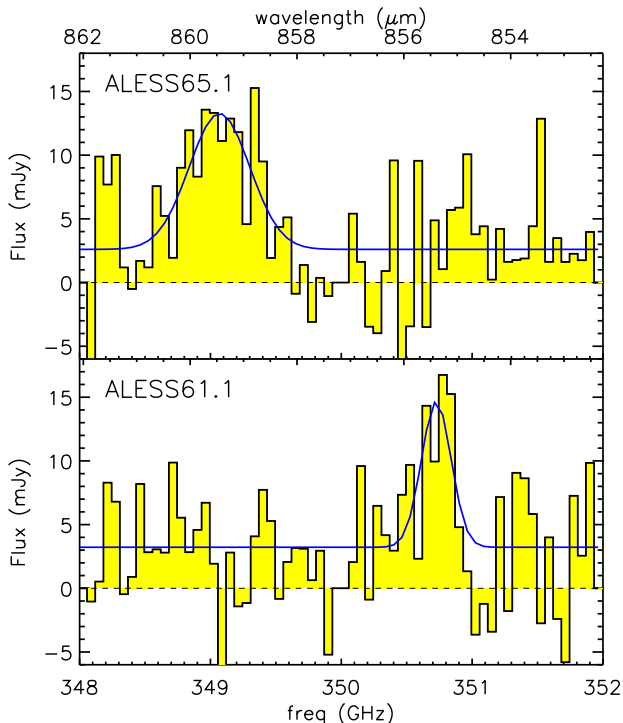


**Figure 3.** ALMA spectra of ALESS 61.1 and ALESS 65.1, extracted at the position of the peak sub-millimetre emission from the SMGs. From the spectra, we identify bright emission lines in the upper side-band which we attribute to [CII] emission at  $z=4.419$  and  $z=4.445$  for ALESS 61.1 and ALESS 65.1, respectively. The rest-frame equivalent widths of the lines are  $0.44 \pm 0.06 \mu\text{m}$  and  $1.12 \pm 0.15 \mu\text{m}$  for ALESS 61.1 and ALESS 65.1 respectively, similar to the median equivalent width of [CII] in local LIRGs and ULIRGs ( $W_{\text{o},[\text{CII}]} = 0.76 \pm 0.06 \mu\text{m}$ ; Brauher et al. 2008). In both cases, due to their selection both SMGs have significant continuum emission.

We caution that there are other possible identifications for these lines. In particular, the emission could also be [OI]  $145 \mu\text{m}$  ( $z \sim 4.9$ ), [NII]  $122 \mu\text{m}$  ( $z \sim 6.0$ ), [NII]  $205 \mu\text{m}$  ( $z \sim 3.1$ ) or much higher redshift, [OIII]  $88 \mu\text{m}$  ( $z \sim 8.1$ ). However, the luminosities of these fine structure lines are expected to be a factor  $\gtrsim 10 \times$  fainter than the [CII] emission (e.g. Brauher et al. 2008; Walter et al. 2009b; Nagao et al. 2012; Decarli et al. 2012).

Alternatively, the emission line could also be high- $J$   $^{12}\text{CO}$  at lower redshift (i.e.  $z = 1.3, 1.6, 2.0$  and  $2.3$  for  $J = 7, 8, 9, 10$  respectively). However, the implied emission line luminosities ( $L = 1-7 \times 10^8 L_{\odot}$ ) are a factor  $\sim 10 \times$  higher than the  $^{12}\text{CO}$  line luminosities of any local or high-redshift starbursts or AGN. For example, Mrk 231 has a maximum  $^{12}\text{CO}$  luminosity (across all  $^{12}\text{CO}$  lines) of  $\lesssim 3 \times 10^7 L_{\odot}$  (van der Werf et al. 2010), whilst APM08279, a well studied high-redshift far-infrared luminous QSO has a  $^{12}\text{CO}(9-8)$  luminosity  $L_{\text{CO}} \lesssim 1 \times 10^8 L_{\odot}$ . Moreover, if the line high- $J$   $^{12}\text{CO}$  (presumably therefore a galaxy with an AGN), then the gas temperature must be high ( $\gtrsim 300$  K if the  $^{12}\text{CO}$  spectral line energy distribution peaks beyond  $J = 7$ ). Yet the characteristic dust temperature would have to be  $\lesssim 15-25$  K (for a dust emissivity of  $\beta = 1.5-2.0$ ). In addition, if these SMGs are lower-redshift ( $z \sim 1-3$ ) starbursts or AGN, then

these SMGs also lie significantly off the far-infrared–radio correlation (Condon et al. 1991; Ivison et al. 2010a).

Taken together, we suggest that the line is most likely a fine structure transition, and given the brightness and equivalent width, probably [CII]. We note that although the redshifts of these two sources are similar ( $\Delta v \sim 1500 \text{ km s}^{-1}$ ), they are separated by 25 arcminutes on the sky (physical distance of 10 Mpc) and so they are not physically associated.

### 3.3 Broad Band Spectral Energy Distribution

We show in Fig. 4 the observed broad-band SED for both galaxies. We overlay the SED of the well-studied  $z = 2.3$  starburst SMM J2135–0102 (Swinbank et al. 2010; Ivison et al. 2010b) redshifted to  $z = 4.4$  and normalised to the  $870 \mu\text{m}$  photometry. This demonstrates that at  $z \sim 4.4$ , the 250, 350 and  $500 \mu\text{m}$  colours and 1.4 GHz of these galaxies are consistent with the expected colours of  $z > 4$  ULIRGs (assuming the properties of ULIRGs at  $z > 4$  are the same as those at  $z \sim 2$ ; Schinnerer et al. 2008; Coppin et al. 2009; Daddi et al. 2009; Capak et al. 2008).

We fit a modified black-body to the far-infrared photometry, deriving estimates of the far-infrared (rest-frame 8–1000  $\mu\text{m}$ ) luminosities of  $L_{\text{FIR}} = (2.1 \pm 0.4) \times 10^{12} L_{\odot}$  and  $L_{\text{FIR}} = (2.0 \pm 0.4) \times 10^{12} L_{\odot}$ , for ALESS 61.1 and ALESS 65.1 respectively (corresponding to star-formation rates of  $\sim 500 M_{\odot} \text{ yr}^{-1}$ ; Kennicutt 1998).

To estimate the near-infrared luminosities of these systems, we use the rest-frame UV–mid-infrared SEDs. We fit elliptical, Sb, single burst and constant star-formation rate spectral templates from Bruzual & Charlot (2003) to the 0.3–8- $\mu\text{m}$  photometry (Table 1 and Fig. 4) using HYPER-Z (Bolzonella et al. 2000) at the known redshift. We allow reddening of  $A_V = 0-5$  in steps of 0.2 and over-plot the best-fitting SED models in Fig. 4. We then calculate the rest-frame  $H$ -band magnitude (observed  $8 \mu\text{m}$  at  $z \sim 4.4$ ), which is less influenced by young stars than rest-frame UV or optical bands and is relatively unaffected by dust. We derive absolute rest-frame  $H$ -band magnitudes of  $H_{\text{AB}} = -24.8 \pm 0.2$  and  $H_{\text{AB}} = -24.2 \pm 0.3$  for ALESS 61.1 and ALESS 65.1, respectively (Table 2). These are comparable to the average  $H$ -band magnitudes for radio-identified sub-millimeter source counterparts at  $z \lesssim 3$  ( $H_{\text{AB}} = -24.1 \pm 0.9$ ; Wardlow et al. 2011), the bulk of which are expected to be SMGs (Smail et al. 2012, in prep).

Owing to the catastrophic degeneracies between star-formation history, age and reddening in SED fitting for dusty sources, to estimate the stellar masses we adopt a simple approach. Following Hainline et al. (2009) and Wardlow et al. (2011) we use the  $H$ -band magnitude together with an average mass-to-light ratio for a likely SMG star-formation history. Hainline et al. (2009) estimate a  $H$ -band mass-to-light ratio for SMGs (with burst and constant star-formation templates), deriving an average  $L_H / M_{\star} \sim 3.8 L_{\odot} / M_{\odot}$  (for a Salpeter IMF). This suggests a stellar mass for ALESS 61.1 and ALESS 65.1 of  $M_{\star} \sim 1.5 \times 10^{11}$  and  $9 \times 10^{10} M_{\odot}$  respectively, comparable to previous estimates for SMG stellar masses (e.g. Hainline et al. 2009; Wardlow et al. 2011). However, we caution that Wardlow et al. (2011) show that the uncertainties in the derived spectral types and ages result in an estimated

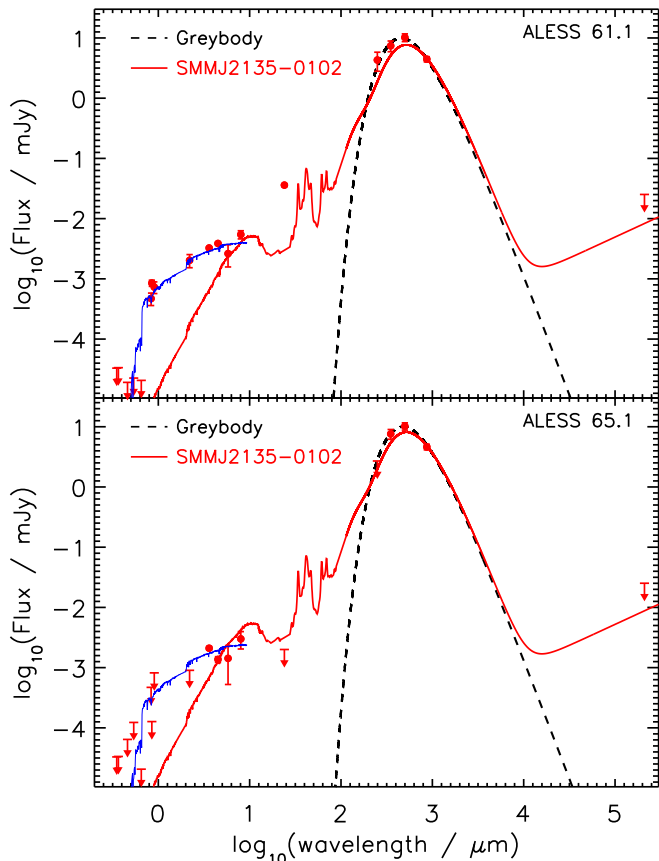


**Figure 4.** The observed optical-radio spectral energy distributions for ALESS 61.1 and ALESS 65.1. We adopt redshifts for the two galaxies of  $z = 4.4189$  and  $z = 4.4445$ . We model the far-infrared SEDs using a single component modified black body dust model (dashed line) by fitting the 250-, 350-, 500- $\mu\text{m}$  limits and 870- $\mu\text{m}$  photometry. We also model the rest-frame UV–near-infrared photometry using HYPER-Z (blue line). The red solid curve shows the SED of the well studied  $z = 2.3$  starburst galaxy, SMM J2135, at the redshift of our galaxies (normalised to the 870- $\mu\text{m}$  flux density). This demonstrates that the far-infrared colours are consistent with the high-redshift nature of these galaxies.

factor of  $\sim 5 \times$  uncertainty in assumed mass-to-light ratios and thus stellar masses.

### 3.4 The [CII] properties

The [CII] luminosities of our two SMGs,  $L_{[\text{CII}]} = 1.5\text{--}3.2 \times 10^9 L_{\odot}$ , are comparable to the luminosities of other high-redshift ULIRGs and QSOs (e.g. Maiolino et al. 2009; Walter et al. 2009a; Wagg et al. 2010; Ivison et al. 2010b; De Breuck et al. 2011; Walter et al. 2012). We can crudely estimate the molecular gas mass for these galaxies using the average [CII]/ $^{12}\text{CO}(1\text{--}0)$  emission line ratio ( $L_{[\text{CII}]} / L_{\text{CO}(1\text{--}0)} = 4400 \pm 1000$ ) from a sample of ten  $z = 2\text{--}4$  starbursts (e.g. Hailey-Dunsheath et al. 2010; Ivison et al. 2010b; Stacey et al. 2010; De Breuck et al. 2011), although we caution that there is significant scatter in the CO/[CII] luminosity ratio (e.g. Fig. 5 of Stacey et al. 2010 shows that there is a range of  $L_{[\text{CII}]} / L_{\text{CO}(1\text{--}0)}$  of approximately 1 dex). Nevertheless, from this compilation of high-redshift observations, the conversion between [CII] line lu-

minosity and molecular gas mass scales approximately as  $M_{\text{gas}} = 10 \pm 2 (L_{[\text{CII}]} / L_{\odot})$ , suggesting a molecular gas mass for these two SMGs of  $M_{\text{gas}} = 1\text{--}4 \times 10^{10} M_{\odot}$ . This molecular gas mass is comparable to the median gas mass implied for SMGs at  $z = 2$ ,  $M_{\text{gas}} = 5 \pm 1 \times 10^{10} M_{\odot}$  (Bothwell et al. 2012). Of course, direct measurements of the low- $J$  CO emission are required to provide a more reliable estimate of the gas mass in these systems.

We can also combine the [CII] and far-infrared luminosities to derive a ratio of  $L_{[\text{CII}]} / L_{\text{FIR}} = (7.1 \pm 1.6) \times 10^{-4}$  and  $(16.0 \pm 3.7) \times 10^{-4}$  for ALESS 61.1 and ALESS 65.1 respectively. As Fig. 5 shows, in local luminous star-forming galaxies the ratio of  $L_{[\text{CII}]} / L_{\text{FIR}}$  declines by a factor  $\sim 100$  over three orders of magnitude in far-infrared luminosity (with a factor  $\sim 3 \times$  scatter at any  $L_{\text{FIR}}$ ). This “[CII] deficit” in local ULIRGs has a number of possible explanations, including enhanced contribution from continuum emission in dusty, high-ionisation regions (Luhman et al. 1998, 2003), high-ionisation effects in the dense environments (Abel et al. 2009) or enhanced contributions to the infrared luminosity from AGN (Sargsyan et al. 2012).

The ratio we derive for the two  $z \sim 4.4$  SMGs is a factor  $\sim 10 \times$  higher than expected for  $z \sim 0$  ULIRGs with their far-infrared luminosity (Fig. 5), although the high  $L_{[\text{CII}]} / L_{\text{FIR}}$  is similar to other high-redshift galaxies of comparable far-infrared luminosity (e.g. Stacey et al. 2010; Cox et al. 2011; Walter et al. 2012). This has been interpreted as evidence that the molecular emission does not reside in a single, compact region illuminated by an intense UV radiation field (as is a good approximation for local ULIRGs), but rather that the [CII] reservoir is more extended, with the high  $L_{[\text{CII}]} / L_{\text{FIR}}$  ratio reflecting the lower density of this extended medium (e.g. Abel et al. 2009; Hailey-Dunsheath et al. 2010; Graciá-Carpio et al. 2011). This interpretation is also consistent with high-resolution studies of SMGs, which have shown that the dust emission and gas reservoirs can be extended over several kilo-parsecs (e.g. Biggs & Ivison 2008; Younger et al. 2008; Tacconi et al. 2008; Ivison et al. 2011; Swinbank et al. 2011) and studies of their mid-infrared colors and spectral properties (Menéndez-Delmestre et al. 2007; Hainline et al. 2009). As we will show in §3.5, the [CII] emission in ALESS 65.1 appears to show velocity structure, and we determine that the [CII] reservoir may be extended across  $\sim 3$  kpc, consistent with this interpretation.

Finally, we note that since the [CII] transition is a primary coolant within the PDRs, it provides a probe of the physical conditions of the gas and interstellar radiation field (e.g. Hollenbach & Tielens 1999; Wolfire et al. 2003). We can therefore use the [CII] and far-infrared luminosity together with the PDR models of Kaufman et al. (1999) to place upper limits on the far-UV radiation field strength and characteristic density of star-forming regions within the ISM. The [CII]/ $L_{\text{FIR}}$  ratio of our two galaxies,  $L_{[\text{CII}]} / L_{\text{FIR}} = 7.1\text{--}16 \times 10^{-4}$ , suggests a mean interstellar far-UV radiation field strength ( $G$ )  $\lesssim 3000 \times$  that of Milky-Way and  $\text{H}_2$  density  $\lesssim 10^{5.5} \text{ cm}^{-3}$  (e.g. Danielson et al. 2011; see also Hailey-Dunsheath et al. 2010 and Stacey et al. 2010). The far-UV field strength limit derived in this way is comparable to that estimated using STARBURST99, which suggests that a  $500 M_{\odot} \text{ yr}^{-1}$  starburst produces a luminosity of  $\sim 5 \times 10^{45} \text{ erg s}^{-1}$  at a wavelength of 1000 Å or

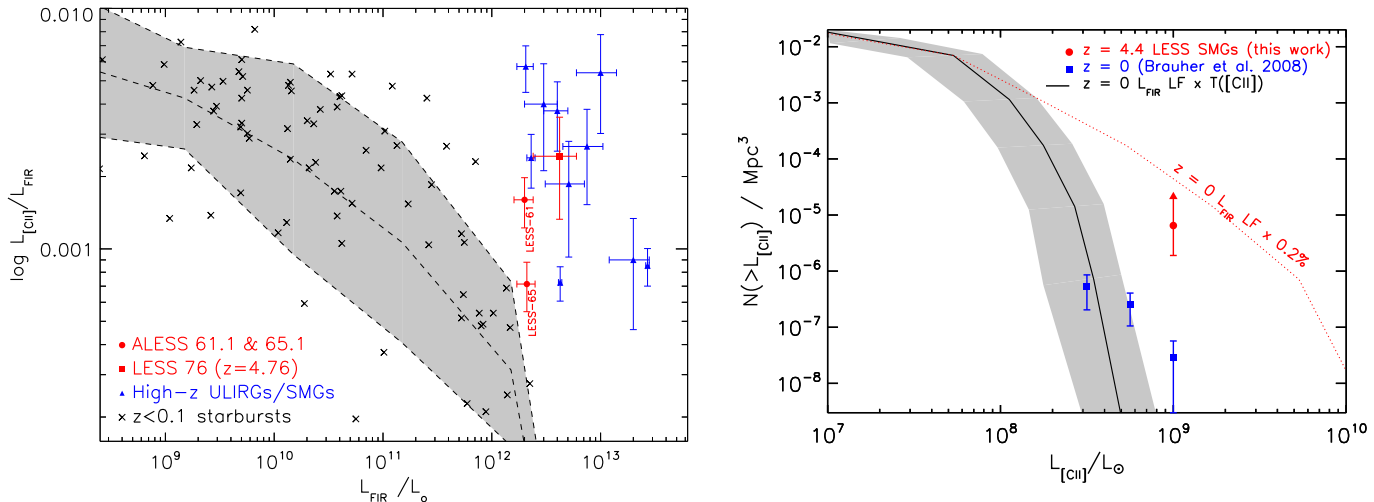


**Figure 5.** *Left:*  $L_{[\text{CII}]} / L_{\text{FIR}}$  ratio as a function of the far-infrared luminosity for our two  $z = 4.4$  ALMA SMGs compared to local star-forming galaxies and ULIRGs. In the plot we also include the  $z = 4.76$  LESS SMG from De Breuck et al. (2011) (see also Coppin et al. 2009). We also include a number of high-redshift starbursts and AGN from previous studies (Malhotra et al. 2001; Colbert et al. 1999; Unger et al. 2000; Spinoglio et al. 2005; Carral et al. 1994; Braucher et al. 2008; Luhman et al. 1998, 2003; Stacey et al. 2010; Cox et al. 2011). For the local data, we calculate the median (dashed line) and scatter (grey). This figure shows that the ratio of  $L_{[\text{CII}]} / L_{\text{FIR}}$  for high-redshift ULIRGs is a factor  $\sim 10 \times$  higher given their far-infrared luminosities compared to those at  $z \sim 0$ . *Right:* The [CII] luminosity function at  $z = 4.4$  from our survey compared to  $z = 0$ . For the  $z = 4.4$  luminosity function, we assume that all of the [CII]-emitting galaxies in the  $\Delta z = 0.12$  volume covered by our observations were detected and so we stress that these calculations yield only a lower-limit on the volume density of high-redshift [CII]-emitters. The  $z = 0$  observations are derived from volume density of *IRAS* sources at  $z < 0.05$  from Braucher et al. (2008). The red dotted line shows the predicted [CII] local luminosity function for a constant  $L_{[\text{CII}]} / L_{\text{FIR}} = 0.002$ , whilst the solid line shows the  $z = 0$  far-infrared luminosity function convolved with the  $L_{[\text{CII}]} / L_{\text{FIR}}$  function from Braucher et al. (2008) (with the grey region denoting the errors in the volume density of local ULIRGs and scatter in the transfer function). Finding two galaxies in this volume probed by our observations indicates a  $\gtrsim 1000$  factor increase in the number density of luminous [CII] emitters from  $z \sim 0$ –4.4, equivalent to a  $\sim 3$ – $4 \times$  [CII] luminosity evolution between  $z = 0$ –4.4.

**Table 2.** Physical Properties of the Galaxies

	ALESS 61.1	ALESS 65.1
$\lambda_c$	$350.726 \pm 0.034 \mu\text{m}$	$349.073 \pm 0.032 \mu\text{m}$
$z_{[\text{CII}]}$	$4.4189 \pm 0.0004$	$4.4445 \pm 0.0005$
$J_{[\text{CII}]}$	$2.5 \pm 0.4 \text{ Jy km s}^{-1}$	$5.4 \pm 0.7 \text{ Jy km s}^{-1}$
FWHM	$230 \pm 25 \text{ km s}^{-1}$	$470 \pm 35 \text{ km s}^{-1}$
$L_{[\text{CII}]}$	$(1.5 \pm 0.3) \times 10^9 L_{\odot}$	$(3.2 \pm 0.4) \times 10^9 L_{\odot}$
$L_{\text{FIR}}$	$(2.1 \pm 0.4) \times 10^{12} L_{\odot}$	$(2.0 \pm 0.4) \times 10^{12} L_{\odot}$
$H_{\text{AB}}$	$-24.8 \pm 0.2$	$-24.2 \pm 0.3$
$L_{\text{H}}$	$(5.9 \pm 1.0) \times 10^{11} L_{\odot}$	$(3.4 \pm 0.8) \times 10^{11} L_{\odot}$
$M_{\star}$	$1.5 \times 10^{11} M_{\odot}$	$9.0 \times 10^{10} M_{\odot}$

Notes: The ALMA data have been primary beam corrected before calculating luminosities. The primary beam corrections are 1.12 and 1.04 for ALESS 61.1 and ALESS 65.1 respectively).

a flux density of  $\sim 10^{3.5} \times$  that of the Milky Way for a source with physical extent of 3 kpc (adopting a far-UV field strength between 912–1103 Å for the Milky Way of  $1.6 \times 10^{-3} \text{ erg s}^{-1} \text{ cm}^{-2}$ ).

### 3.5 Internal structure

Given the spatial resolution of our observations ( $\sim 1.4''$  FWHM), we search for spatially resolved emission and velocity structure within these two SMGs. From the ALMA data of LESS 65, the total flux of the galaxy

( $S_{870} = 4.24 \pm 0.49 \text{ mJy}$ ) is marginally higher than the peak flux in the map ( $S_{\text{peak}} = 3.60 \pm 0.49 \text{ mJy beam}^{-1}$ ) indicating that the source may be marginally resolved. Using the [CII] emission in this galaxy, we examine whether there is any evidence for velocity structure by comparing the spatial distribution of the integrated [CII] emission between  $-210$ – $0 \text{ km s}^{-1}$  and  $0$ – $210 \text{ km s}^{-1}$  (i.e.  $\pm$ FWHM relative to the systemic redshift in the continuum subtracted cube). By centroiding the two maps we derive a spatial offset of  $3.3 \pm 1.7 \text{ kpc}$  between the redshifted and blue-shifted emission (Fig. 1). Although tentative, this spatial extent is similar to the [CII] spatial extent of the bright  $z \sim 5$  SMG HDF 850.1 where similar data are available (Walter et al. 2012), and also to the high- $J$   $^{12}\text{CO}$  molecular emission FWHM ( $\sim 4 \text{ kpc}$ ) from a sample of eight SMGs at  $z \sim 2$  (Tacconi et al. 2006). If the spatial offset in ALESS 65.1 represents rotating gas, then we estimate a mass  $M_{\text{dyn}} \sim 3.5 \times 10^{10} \sin^2(i)$ , which is consistent with the implied gas and stellar mass estimates.

### 3.6 The evolution of the [CII] luminosity function

Since our ALMA survey has followed up *all* of the LESS SMGs, we can use the detection rate to investigate the evolution of the [CII] luminosity function. In the following we assume that all of the [CII]-emitting galaxies in the  $\Delta z = 0.12$  volume covered by our observations were detected and so we stress that these calculations yield only a lower-limit on the volume density of high-redshift [CII]-emitters.

To estimate the  $z \sim 0$  [CII] luminosity function, we start from the  $z \sim 0$  far-infrared luminosity function of Sanders et al. (2003) and initially assume a constant  $L_{[\text{CII}]} / L_{\text{FIR}} = 0.002$  (Fig. 5). This provides a firm upper limit to the bright end of  $z \sim 0$  [CII] luminosity function, given the observed decline in  $L_{[\text{CII}]} / L_{\text{FIR}}$  at high  $L_{\text{FIR}}$  (Fig. 5). We can then use the correlation of  $L_{[\text{CII}]} / L_{\text{FIR}}$  with  $L_{\text{FIR}}$  from Brauher et al. (2008) (see also Fig. 5) to provide a more reliable estimate. We show our best estimate of the  $z \sim 0$  [CII] luminosity function in Fig. 5, including the expected dispersion due to the scatter in the local  $L_{[\text{CII}]} / L_{\text{FIR}} - L_{\text{FIR}}$  relation.

To assess the reliability of this  $z \sim 0$  [CII] luminosity function we attempt to independently derive this using the Brauher et al. (2008) study of [CII] emission in a sample of 227  $z < 0.05$  galaxies from the *ISO* archive. The parent population of this study can be approximated by an *IRAS* 100- $\mu\text{m}$  selected sample at  $z < 0.05$  with flux densities between  $S_{100\mu\text{m}} = 1\text{--}1000$  Jy. There are  $\sim 11,000$  *IRAS* sources within this redshift and flux density range and so we must account for the incompleteness in the Brauher et al. (2008) sample to derive the  $z \sim 0$  [CII] luminosity function. We start by assuming the Brauher et al. (2008) sample is a random subset of the parent population (although we note it is likely that apparently bright sources are over-represented in the sample, and fainter sources correspondingly under-represented). We then only consider *IRAS* sources with flux densities  $> 10$  Jy where the fraction of galaxies observed in the Brauher et al. (2008) sample is  $\gtrsim 3\%$  of the parent population and then calculate the fraction of galaxies in the Brauher et al. (2008) sample compared to the number of *IRAS* galaxies at  $z < 0.05$  in bins of 100- $\mu\text{m}$  flux density and redshift. We use these sampling fractions to correct the apparent [CII] luminosity function within  $z < 0.05$  (a comoving volume of  $0.035 \text{ Gpc}^3$ ) and show these data in Fig. 5.

Whilst the local data from Brauher et al. (2008) comprise a complex mix of observations derived from a number of studies, the data are broadly consistent with the bright end of the  $z \sim 0$  [CII] luminosity function we derived above from the far-infrared luminosity function and  $L_{[\text{CII}]} / L_{\text{FIR}}$  transfer function.

To place the new ALMA-identified  $z = 4.4$  SMGs on this plot, we estimate the volume covered by our observations of ECDFS by considering that the brightest [CII] emitters will correspond to the brightest far-infrared sources (i.e. SMGs). The LESS SMGs are located within a  $0.5^\circ \times 0.5^\circ$  region and assuming our ALMA observations cover the [CII] with a redshift range of  $\Delta z = 0.12$  at  $z \sim 4.4$ , we derive a comoving volume of  $2.9 \times 10^5 \text{ Mpc}^3$ . Finding two galaxies in this volume with [CII] luminosities  $> 1 \times 10^9 L_\odot$  indicates a  $\gtrsim 1000$  factor increase in the number density of luminous [CII] emitters from  $z \sim 0\text{--}4.4$ . This is equivalent to a  $\sim 3\text{--}4 \times$  [CII] luminosity evolution between  $z = 0\text{--}4.4$  which is consistent with the evolution in the far-infrared luminosity function (factor  $\sim 3 \times$  in  $L_{\text{FIR}}$  for a fixed volume density of  $\phi = 10^{-5} \text{ Mpc}^{-1}$ ; Wardlow et al. 2011) between  $z = 0$  and  $z = 3$ , although since the far-infrared luminosity function declines beyond  $z = 3$ , the [CII] luminosity function may peak at lower redshift than probed by our observations here.

## 4 SUMMARY

We have undertaken an ALMA study of 126 sub-millimetre sources from the LABOCA 870 $\mu\text{m}$  survey of the ECDFS (Weiß et al. 2009). We focus here on two high-redshift SMGs that are precisely located by our high resolution ALMA continuum observations and whose ALMA spectra detect bright emission lines. We interpret these lines as the far-infrared atomic fine structure line [CII] 157.74, indicating redshifts of  $z = 4.4$  for both galaxies. We show that the ratio of  $L_{[\text{CII}]} / L_{\text{FIR}}$  is higher than comparably luminous galaxies at  $z = 0$ , but consistent with the ratio seen in other high-redshift ULIRGs. We interpret this as evidence that the molecular emission is extended and indeed, in one of our SMGs our data suggest that the [CII] is resolved on  $\gtrsim 3 \text{ kpc}$  scales. Given the volume probed by our observations, we show that the [CII] luminosity function must evolve strongly across the 12 Gyrs between  $z = 0$  and  $z \sim 4$ .

These results show that the wide spectral baseline coverage of ALMA provides the opportunity to measure blind redshifts of large samples of distant, obscured galaxies through the detection of fine structure emission lines, such as [CII], in short exposure times.

## ACKNOWLEDGMENTS

We would like to thank the anonymous referee for a thoughtful and constructive report which improved the content and clarity of this paper. The ALMA observations were carried out under program 2011.0.00294.S. ALMA is a partnership of ESO (representing its member states), NSF (USA) and NINS (Japan), together with NRC (Canada) and NSC and ASIAA (Taiwan), in cooperation with the Republic of Chile. The Joint ALMA Observatory is operated by ESO, AUI/NRAO and NAOJ. This publication is also based on data acquired with the APEX under programme IDs 078.F-9028(A), 079.F-9500(A), 080.A-3023(A) and 081.F-9500(A). APEX is a collaboration between the Max-Planck-Institut für Radioastronomie, the European Southern Observatory and the Onsala Space Observatory. This research also made use of data from the HerMES Key Programme from the SPIRE instrument team, ESAC scientists and a mission scientist. Herschel is an ESA space observatory with science instruments provided by European-led Principal Investigator consortia and with important participation from NASA. AMS gratefully acknowledges an STFC Advanced Fellowship. IRS acknowledges support from STFC and a Leverhulme Fellowship. KEKC acknowledges support from the endowment of the Lorne Trottier Chair in Astrophysics and Cosmology at McGill, the Natural Science and Engineering Research Council of Canada (NSERC), and a L'Oréal Canada for Women in Science Research Excellence Fellowship, with the support of the Canadian Commission for UNESCO. TRG acknowledges the Science and Technologies Facilities Council as well as IDA and DARK.

## REFERENCES

- Abel, N. P., Dudley, C., Fischer, J., Satyapal, S., & van Hoof, P. A. M. 2009, *ApJ*, 701, 1147
- Biggs, A. D. & Ivison, R. J. 2008, *MNRAS*, 385, 893



- Biggs, A. D., Ivison, R. J., Ibar, E., Wardlow, J. L., Dannerbauer, H., Smail, I., Walter, F., & Weiß, A. et al. 2011, *MNRAS*, 413, 2314
- Blain, A. W., Smail, I., Ivison, R. J., & Kneib, J.-P. 1999, *MNRAS*, 302, 632
- Blain, A. W., Smail, I., Ivison, R. J., Kneib, J.-P., & Frayer, D. T. 2002, *PhR*, 369, 111
- Bolzonella, M., Miralles, J.-M., & Pelló, R. 2000, *A&A*, 363, 476
- Bothwell, M. S., Smail, I., Chapman, S. C., Genzel, R., Ivison, R. J., Tacconi, L. J., Alaghband-Zadeh, S., & Bertoldi, F. et al. 2012, *ArXiv e-prints*
- Brauher, J. R., Dale, D. A., & Helou, G. 2008, *ApJS*, 178, 280
- Bruzual, G. & Charlot, S. 2003, *MNRAS*, 344, 1000
- Capak, P., Carilli, C. L., Lee, N., Aldcroft, T., Aussel, H., Schinnerer, E., Wilson, G. W., & Yun, M. S. et al. 2008, *ApJL*, 681, L53
- Carilli, C. L. & Yun, M. S. 2000, *ApJ*, 530, 618
- Carral, P., Hollenbach, D. J., Lord, S. D., Colgan, S. W. J., Haas, M. R., Rubin, R. H., & Erickson, E. F. 1994, *ApJ*, 423, 223
- Chapman, S. C., Blain, A. W., Smail, I., & Ivison, R. J. 2005, *ApJ*, 622, 772
- Chapman, S. C., Smail, I., Windhorst, R., Muxlow, T., & Ivison, R. J. 2004, *ApJ*, 611, 732
- Colbert, J. W., Malkan, M. A., Clegg, P. E., Cox, P., Fischer, J., Lord, S. D., Luhman, M., & Satyapal, S. et al. 1999, *ApJ*, 511, 721
- Condon, J. J., Anderson, M. L., & Helou, G. 1991, *ApJ*, 376, 95
- Coppin, K. E. K., Smail, I., Alexander, D. M., Weiss, A., Walter, F., Swinbank, A. M., Greve, T. R., Kovacs, A., & De Breuck, C. et al. 2009, *MNRAS*, 395, 1905
- Cox, P., Krips, M., Neri, R., Omont, A., Güsten, R., Menten, K. M., Wyrowski, F., & Weiß, A. et al. 2011, *ApJ*, 740, 63
- Daddi, E., Dannerbauer, H., Krips, M., Walter, F., Dickinson, M., Elbaz, D., & Morrison, G. E. 2009, *ApJL*, 695, L176
- Danielson, A. L. R., Swinbank, A. M., Smail, I., Cox, P., Edge, A. C., Weiss, A., Harris, A. I., & Baker, A. J. et al. 2011, *MNRAS*, 410, 1687
- Dannerbauer, H., Lehnert, M. D., Lutz, D., Tacconi, L., Bertoldi, F., Carilli, C., Genzel, R., & Menten, K. 2002, *ApJ*, 573, 473
- De Breuck, C., Maiolino, R., Caselli, P., Coppin, K., Hailey-Dunsheath, S., & Nagao, T. 2011, *A&A*, 530, L8
- Decarli, R., Walter, F., Neri, R., Bertoldi, F., Carilli, C., Cox, P., Kneib, J. P., & Lestrade, J. F. et al. 2012, *ApJ*, 752, 2
- Frayer, D. T., Smail, I., Ivison, R. J., & Scoville, N. Z. 2000, *AJ*, 120, 1668
- Gear, W. K., Lilly, S. J., Stevens, J. A., Clements, D. L., Webb, T. M., Eales, S. A., & Dunne, L. 2000, *MNRAS*, 316, L51
- Graciá-Carpio, J., Sturm, E., Hailey-Dunsheath, S., Fischer, J., Contursi, A., Poglitsch, A., Genzel, R., & et al., G. 2011, *ApJL*, 728, L7
- Hailey-Dunsheath, S., Nikola, T., Stacey, G. J., Oberst, T. E., Parshley, S. C., Benford, D. J., Staguhn, J. G., & Tucker, C. E. 2010, *ApJL*, 714, L162
- Hailey-Dunsheath, S., Nikola, T., Stacey, G. J., Oberst, T. E., Parshley, S. C., Bradford, C. M., Ade, P. A. R., & Tucker, C. E. 2008, *ApJL*, 689, L109
- Hainline, L. J., Blain, A. W., Smail, I., Frayer, D. T., Chapman, S. C., Ivison, R. J., & Alexander, D. M. 2009, *ApJ*, 699, 1610
- Hollenbach, D. J. & Tielens, A. G. G. M. 1999, *Reviews of Modern Physics*, 71, 173
- Ivison, R. J., Greve, T. R., Dunlop, J. S., Peacock, J. A., Egami, E., Smail, I., & Ibar et al. 2007, *MNRAS*, 380, 199
- Ivison, R. J., Greve, T. R., Smail, I., Dunlop, J. S., Roche, N. D., Scott, S. E., Page, M. J., & Stevens et al. 2002, *MNRAS*, 337, 1
- Ivison, R. J., Harrison, A. P., & Coulson, I. M. 1998, *A&A*, 330, 443
- Ivison, R. J., Magnelli, B., Ibar, E., Andreani, P., Elbaz, D., Altieri, B., Amblard, A., & Arumugam, V. et al. 2010a, *A&A*, 518, L31
- Ivison, R. J., Papadopoulos, P. P., Smail, I., Greve, T. R., Thomson, A. P., Xilouris, E. M., & Chapman, S. C. 2011, *MNRAS*, 412, 1913
- Ivison, R. J., Swinbank, A. M., Swinyard, B., Smail, I., Pearson, C. P., Rigopoulou, D., Polehampton, E., & Baluteau, J.-P. et al. 2010b, *A&A*, 518, L35
- Kaufman, M. J., Wolfire, M. G., Hollenbach, D. J., & Luhman, M. L. 1999, *ApJ*, 527, 795
- Kennicutt, R. C. 1998, *ARAA*, 36, 189
- LeFloc'h, E., Aussel, H., Ilbert, O., Riguccini, L., Frayer, D. T., Salvato, M., Arnouts, S., & Surace, J. et al. 2009, *ApJ*, 703, 222
- Lindner, R. R., Baker, A. J., Omont, A., Beelen, A., Owen, F. N., Bertoldi, F., Dole, H., & Fiolet, N. et al. 2011, *ApJ*, 737, 83
- Lord, S. D., Malhotra, S., Lim, T., Helou, G., Rubin, R. H., Stacey, G. J., Hollenbach, D. J., & Werner, M. W. et al. 1996, *A&A*, 315, L117
- Luhman, M. L., Satyapal, S., Fischer, J., Wolfire, M. G., Cox, P., Lord, S. D., Smith, H. A., Stacey, G. J., & Unger, S. J. 1998, *ApJL*, 504, L11
- Luhman, M. L., Satyapal, S., Fischer, J., Wolfire, M. G., Sturm, E., Dudley, C. C., Lutz, D., & Genzel, R. 2003, *ApJ*, 594, 758
- Madden, S. C., Geis, N., Genzel, R., Herrmann, F., Jackson, J., Poglitsch, A., Stacey, G. J., & Townes, C. H. 1993, *ApJ*, 407, 579
- Maiolino, R., Caselli, P., Nagao, T., Walmsley, M., De Breuck, C., & Meneghetti, M. 2009, *A&A*, 500, L1
- Maiolino, R., Cox, P., Caselli, P., Beelen, A., Bertoldi, F., Carilli, C. L., Kaufman, M. J., & Menten, K. M. et al. 2005, *A&A*, 440, L51
- Malhotra, S., Kaufman, M. J., Hollenbach, D., Helou, G., Rubin, R. H., Brauher, J., Dale, D., & Lu, N. Y. et al. 2001, *ApJ*, 561, 766
- McMullin, J. P., Waters, B., Schiebel, D., Young, W., & Golap, K. 2007, in *Astronomical Society of the Pacific Conference Series*, Vol. 376, *Astronomical Data Analysis Software and Systems XVI*, ed. R. A. Shaw, F. Hill, & D. J. Bell, 127
- Menéndez-Delmestre, K., Blain, A. W., Alexander, D. M., Smail, I., Armus, L., Chapman, S. C., Frayer, D. T., Ivison, R. J., & Teplitz, H. I. 2007, *ApJL*, 655, L65
- Nagao, T., Maiolino, R., De Breuck, C., Caselli, P., Hat-

- sukade, B., & Saigo, K. 2012, eprint arXiv:1205.4834
- Pope, A., Scott, D., Dickinson, M., Chary, R.-R., Morrison, G., Borys, C., Sajina, A., & Alexander, D. et al. 2006, *MNRAS*, 370, 1185
- Sakamoto, K., Wang, J., Wiedner, M. C., Wang, Z., Peck, A. B., Zhang, Q., Petitpas, G. R., & Ho, L., et al. 2008, *ApJ*, 684, 957
- Sanders, D. B., Mazzarella, J. M., Kim, D.-C., Surace, J. A., & Soifer, B. T. 2003, *AJ*, 126, 1607
- Sanders, D. B. & Mirabel, I. F. 1996, *ARAA*, 34, 749
- Sargsyan, L., Leboutellier, V., Weedman, D., Spoon, H., Bernard-Salas, J., Engels, D., Stacey, G., Houck, J., Barry, D., Miles, J., & Samsonyan, A. 2012, *ArXiv e-prints*
- Schinnerer, E., Carilli, C. L., Capak, P., Martinez-Sansigre, A., Scoville, N. Z., Smolčić, V., Taniguchi, Y., Yun, M. S., Bertoldi, F., Le Fevre, O., & de Ravel, L. 2008, *ApJL*, 689, L5
- Smail, I., Swinbank, A. M., Ivison, R. J., & Ibar, E. 2011, *MNRAS*, 414, L95
- Smolčić, V., Navarrete, F., Aravena, M., Ilbert, O., Yun, M. S., Sheth, K., Salvato, M., & McCracken, H. J. et al. 2012, *ApJS*, 200, 10
- Spinoglio, L., Malkan, M. A., Smith, H. A., González-Alfonso, E., & Fischer, J. 2005, *ApJ*, 623, 123
- Stacey, G. J., Geis, N., Genzel, R., Lugten, J. B., Poglitsch, A., Sternberg, A., & Townes, C. H. 1991, *ApJ*, 373, 423
- Stacey, G. J., Hailey-Dunsheath, S., Ferkinhoff, C., Nikola, T., Parshley, S. C., Benford, D. J., Staguhn, J. G., & Fiolet, N. 2010, *ApJ*, 724, 957
- Swinbank, A. M., Papadopoulos, P. P., Cox, P., Krips, M., Ivison, R. J., Smail, I., Thomson, A. P., Neri, R., Richard, J., & Ebeling, H. 2011, *ApJ*, 742, 11
- Swinbank, A. M., Smail, I., Longmore, S., Harris, A. I., Baker, A. J., De Breuck, C., Richard, J., & Edge, A. C. et al. 2010, *Nature*, 464, 733
- Tacconi, L. J., Genzel, R., Smail, I., Neri, R., Chapman, S. C., Ivison, R. J., Blain, A., & Cox, P., et al. 2008, *ApJ*, 680, 246
- Tacconi, L. J., Neri, R., Chapman, S. C., Genzel, R., Smail, I., Ivison, R. J., Bertoldi, F., & Blain et al. 2006, *ApJ*, 640, 228
- Unger, S. J., Clegg, P. E., Stacey, G. J., Cox, P., Fischer, J., Greenhouse, M., Lord, S. D., & Luhman, M. L. et al. 2000, *A&A*, 355, 885
- Valtchanov, I., Virdee, J., Ivison, R. J., Swinbank, B., van der Werf, P., Rigopoulou, D., da Cunha, E., & Lupu R. et al. 2011, *MNRAS*, 415, 3473
- van der Werf, P. P., Isaak, K. G., Meijerink, R., Spaans, M., Rykala, A., Fulton, T., Loenen, A. F., & Walter, F. et al. 2010, *A&A*, 518, L42
- Wagg, J., Carilli, C. L., Wilner, D. J., Cox, P., De Breuck, C., Menten, K., Riechers, D. A., & Walter, F. 2010, *A&A*, 519, L1
- Walter, F., Decarli, R., Carilli, C., Bertoldi, F., Cox, P., da Cunha, E., Daddi, E., & Dickinson, M. et al. 2012, *Nature*, 486, 233
- Walter, F., Riechers, D., Cox, P., Neri, R., Carilli, C., Bertoldi, F., Weiss, A., & Maiolino, R. 2009a, *Nature*, 457, 699
- Walter, F., Weiß, A., Riechers, D. A., Carilli, C. L., Bertoldi, F., Cox, P., & Menten, K. M. 2009b, *ApJL*, 691, L1
- Wang, W.-H., Cowie, L. L., Barger, A. J., & Williams, J. P. 2011, *ApJL*, 726, L18
- Wardlow, J. L., Smail, I., Coppin, K. E. K., Alexander, D. M., Brandt, W. N., Danielson, A. L. R., Luo, B., & Swinbank, A. M. et al. 2011, *MNRAS*, 415, 1479
- Weiß, A., Kovács, A., Coppin, K., Greve, T. R., Walter, F., Smail, I., Dunlop, J. S., & Knudsen, K. K. et al. 2009, *ApJ*, 707, 1201
- Wolfire, M. G., McKee, C. F., Hollenbach, D., & Tielens, A. G. G. M. 2003, *ApJ*, 587, 278
- Younger, J. D., Fazio, G. G., Huang, J.-S., Yun, M. S., Wilson, G. W., Ashby, M. L. N., Gurwell, M. A., & Lai et al. 2007, *ApJ*, 671, 1531
- Younger, J. D., Fazio, G. G., Wilner, D. J., Ashby, M. L. N., Blundell, R., Gurwell, M. A., Huang, J.-S., & Iono, D. et al. 2008, *ApJ*, 688, 59